A comparative study on effects of cone-plate and parallel-plate geometries on rheological properties under oscillatory shear flow

Hyeong Yong Song[1], Reza Salehiyan[2], Xiaolei Li[1], Seung Hak Lee[1] and Kyu Hyun[1,*]

[1]*School of Chemical and Biomolecular Engineering, Pusan National University, Busan 46241, Republic of Korea*

[2]*DST-CSIR National Centre for Nanostructured Materials, Council for Scientific and Industrial Research, Pretoria 0001, South Africa*

*Corresponding author; E-mail: kyuhyun@pusan.ac.kr

ABSTRACT: This paper investigates effects of cone-plate (CP) and parallel-plate (PP) geometries on rheological properties of various complex fluids from single-phase to multiphase systems. Small amplitude oscillatory shear (SAOS) tests were carried out to compare linear rheological responses while nonlinear responses were compared via large amplitude oscillatory shear (LAOS) tests at different frequencies. Moreover, Fourier-transform (FT) rheology method was used to analyze the nonlinear responses under LAOS flow. Experimental results were compared with the predictions by a single-point correction and a shear rate correction. For all systems, SAOS data measured by CP and PP coincide with each other. Discordance between CP and PP measurements is observed in nonlinear regime. For all systems except xanthan gum solutions, first-harmonic moduli are corrected by a single horizontal shift factor and FT-based nonlinear parameters ($I_{3/1}$, Q_3, $I_{5/1}$, and Q_5) are corrected by vertical shift factors which are predicted well by a single-point correction. Xanthan gum solutions exhibit anomalous corrections. Their first-harmonic Fourier moduli are superposed by a horizontal shift factor predicted by a shear rate correction which is applicable to highly shear-thinning fluids. The distinguished corrections are observed in FT-based nonlinear parameters. $I_{3/1}$ and $I_{5/1}$ are superposed by horizontal shifts while the other systems display vertical shifts of $I_{3/1}$ and

$I_{5/1}$. Q_3 and Q_5 of xanthan gum solutions are corrected by both horizontal and vertical shift factors. In particular, the obtained vertical shift factors for Q_3 and Q_5 are two times larger than the predictions by a single-point correction. Such larger values are rationalized by the definitions of Q_3 and Q_5. These results highlight the significance of horizontal shift corrections in nonlinear oscillatory shear data.

***Keywords*:** parallel plate, cone plate, LAOS, FT-rheology, shift factor

1. Introduction

Studying rheological properties of complex fluids is of many scientists' interests in order to investigate and characterize flow behaviors of diverse materials with different morphologies. Morphology dependence of rheological properties has led to more systematic investigation of rheological properties of various complex fluids having different internal structures from single-phase to multi-phase fluids. Dynamic oscillatory shear tests are being mainly used to study the viscoelastic behavior of polymer solutions and melts. Hence, rotational rheometers are used to perform dynamic oscillatory experiments (Djalili-Moghaddam *et al.*, 2004). Different geometries can be used in case of rotational rheometers, among which parallel plate, cone plate and concentric cylinder are the most common. In this study, a comparative examination of rheological properties from cone-plate (CP) and parallel-plate (PP) fixtures was conducted. Schematic views of both parallel-plate (PP) and cone-plate (CP) geometries are sketched in Fig. 1. Mathematical equations describing viscoelastic properties corresponding to PP and CP geometries are summarized in Table 1, where θ is cone angle, T is torque, Ω is angular velocity, R is plate radius, and h is the gap size between two plates while viscosity η is considered constant (Bohlin *et al.*, 1980; Djalili-Moghaddam *et al.*, 2004; Kavehpour and McKinley, 2004; Macosko, 1994). The subscript R in the equation for shear rate in the PP geometry indicates the rim shear rate at the edge of the plate (radius R).

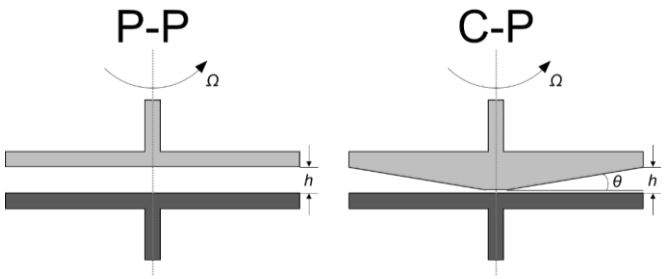

Fig. 1. Schematic views of torsional parallel-plate (PP) and cone-plate (CP) geometries for rheological measurements.

Table 1. Working equations for parallel-plate (PP) and cone-plate (CP) geometries.

	Parallel plate	Cone plate
Torque	$T = \frac{\pi\Omega\eta R^4}{2h}$	$T = \frac{2\pi\Omega\eta R^3}{3\tan\theta}$
Stress	$\sigma = \frac{T}{2\pi R^3}\left[3 + \frac{d\ln T}{d\ln\dot{\gamma}_R}\right]$	$\sigma = \frac{3T}{2\pi R^3}$
Shear rate	$\dot{\gamma}_R = \frac{\Omega R}{h}$	$\dot{\gamma} = \frac{\Omega}{\tan\theta}$

PP fixtures have the privilege of feasible varying the gap size, leading to application of various ranges of materials, which is impossible in a fixed-gap CP geometry. Sample preparation and loading is simpler in PP geometry for rigid viscoelastic materials or irreversible gels. Moreover, larger strains can be applied in PP because it is simpler geometry. On the other hand, CP fixtures can be used to determine first normal force difference as shear stress and shear rate are constant throughout the gap while in case of PP geometry they exhibit maximum value at the edge of the geometry and zero value along the vertical axis, that is, a radially inhomogeneous flow field. This produces a uniform strain field in CP fixture and a non-uniform

strain field in PP fixture, respectively. For utility and errors of each geometry in detail, see Macosko (1994).

Several studies carried out to assess geometry effects on rheological properties. Lodge (1961) conducted an experiment to evaluate wedge effects for both CP and PP fixtures through the measurement of pressure distributions. In order to obtain more precise wedge effects, the fixed plate was designed in a way which could be easily tilted about horizontal axis to get the intended angles with pressure measuring holes. It was found that both CP and PP geometries exhibit similar pressure distributions perpendicular along the greatest slope. However, the greatest pressure took place near the rotational axis in CP fixture and was three times greater than that of PP fixture. Accordingly, the wedge effect was found to be twelve times greater in CP than that of PP. Keentok and Tanner (1982) compared the normal stresses obtained from CP and PP for two different polymer solutions and observed greater normal stresses in PP than that of CP at the same shear rates. Djalili-Moghaddam *et al.* (2004) compared the results of CP and PP geometries for suspensions of polydimethylsiloxane (PDMS) using steady shear measurements at two different stress levels. They found that PP geometry yields to higher values of viscosities than CP geometry regardless of stress levels. They suggested that the generated non-uniform shear flow in PP geometry produced higher viscosities than that of CP geometry. Egres and Wagner (2005) applied stress sweep measurements to compare the effect of different geometries of PP, CP, and Couette cell on suspensions of polyethylene glycol/precipitated calcium carbonate (PEG/PCC). A good agreement was observed in case of CP and Couette cell geometries. PP fixture resulted in lower values at higher stress amplitude. It was demonstrated that wall slip effect could be the reason for this reduction in PP geometry. Shaw and Liu (2006) carried out an experiment to compare the linear and nonlinear rheological data from CP and PP for poly[styrene-*b*-(ethylene-*ran*-propylene)] (SEP) block copolymer in

squalane (saturated isoprene oligomer). Dynamic and steady measurements were used to evaluate the rheological properties. They also introduced single-point and conventional corrections to the PP equations to get the best fitted data with CP data. Surprisingly, both steady and dynamic results showed a mismatch fit. They attributed this mismatch to gap setting problems.

The mismatch in rheological properties obtained by CP and PP geometries is no exception for large amplitude oscillatory shear (LAOS) test. For strain-controlled LAOS test (LAOStrain) (Ewoldt, 2013), typical strain sweep data is divided into linear and nonlinear regimes (Hyun *et al.*, 2011). In linear regime, dynamic moduli (G' and G'') are independent of strain amplitude. As strain amplitude increases and moves toward nonlinear regime, the moduli decrease and become a function of strain amplitude. Many literatures show consistency of linear viscoelastic moduli between the two geometries and imply that no correction is required in the linear regime while mismatch occurs in the nonlinear regime (Bharadwaj and Ewoldt, 2015; de Souza Mendes *et al.*, 2014; Shaw and Liu, 2006; Stickel *et al.*, 2013). Inconsistency between PP and CP geometries is due to different degree of nonlinear intensities generated by existence of higher harmonics in nonlinear stress signal. Thus, it is important to quantify nonlinearities of LAOS response obtained by CP and PP and to correct difference between the two geometries by proper methods.

Wilhelm *et al.* (1999) introduced highly sensitive Fourier-transform (FT) rheology as a new way to characterize nonlinearities. The ratio of the third harmonic intensity to the fundamental intensity ($I(3\omega)/I(\omega) \equiv I_{3/1}$, ω is applied frequency) was considered as a new characterization parameter to quantify nonlinearities. They evaluated the influence of different shear geometries. The horizontal shift factor of 0.75 was used to compensate for the difference of two geometries, which is the ratio of the characteristic radius of PP geometry to the total radius. At the

characteristic radius of PP geometry, the shear rate in the linear regime is similar to that of CP geometry (Macosko, 1994). It was observed that the shift factor of 0.75 was able to improve the differences between PP and CP. However, the usage of this horizontal shift factor did not result in absolutely identical superposition, especially at large strain amplitude, indicating that a single 0.75 factor may not be proper to perfectly match two data. Recently, several new nonlinear parameters have been suggested based on the dependency of nonlinear shear stresses on strain amplitude: a nonlinear mechanical parameter $Q(\omega, \gamma_0) \equiv I_{3/1}/\gamma_0^2$, an intrinsic nonlinearity $Q_0(\omega) \equiv \lim_{\gamma_0 \to 0} Q(\omega, \gamma_0)$, and four intrinsic Chebyshev coefficients $[e_1](\omega)$, $[v_1](\omega)$, $[e_3](\omega)$, and $[v_3](\omega)$ (Ewoldt and Bharadwaj, 2013; Hyun and Wilhelm, 2009). They are asymptotically-nonlinear measures defined in medium amplitude oscillatory shear (MAOS) regime where the third harmonic nonlinearity is dominant and the other higher harmonics can be ignored. Several approaches have been used to compensate for effects of inhomogeneous strain condition in PP geometry on these nonlinear coefficients. Wagner *et al.* (2011) calculated a vertical shift factor of 3/2 for fluids with nonlinear shear stress conforming to the power-law series expansion in odd powers. The same shift factor was obtained from single-mode corotational Maxwell model (Giacomin *et al.*, 2015). Bharadwaj and Ewoldt (2015) used a general single-point correction for four intrinsic Chebyshev measures, which also results in the same vertical shift factor of 3/2. Therefore, it is speculated that all MAOS nonlinear properties in PP geometry can be balanced by 3/2 correction factor to obtain the values in CP one.

The object of this paper is to compare the linear and nonlinear viscoelastic behaviors of various polymer systems from single-phase to multiphase systems such as homopolymer melts and solutions, blends, and nanocomposites for PP and CP geometries. In addition, the shift factors from experiments were compared with the theoretical prediction by single-point correction and shear rate correction. We show that the predicted value matches experimental

results for all systems. Our results suggest usage and utility of horizontal shift factor as well as those of vertical shift factor for perfect superposition of CP and PP measurements.

2. Theory

In this work, a general single-point correction was used to compensate for strain-controlled LAOS response measured by PP geometry. A single-point correction approach has been applied to various test conditions such as large step shear (Soskey and Winter, 1984), steady shear (Carvalho *et al.*, 1994), start-up shear (Shaw and Liu, 2006), and creep (de Souza Mendes *et al.*, 2014) as well as LAOS (Bharadwaj and Ewoldt, 2015; Fahimi *et al.*, 2014; Ng *et al.*, 2011; Phan-Thien *et al.*, 2000). Ng *et al.* (2011) derived a single-point correction for LAOS response based on earlier correction methods as follows:

$$\sigma_c(t;\omega,\gamma_0)=\frac{3}{4}\sigma_p(t;\omega,\gamma_0)+\frac{\gamma_0}{4}\frac{\partial}{\partial\gamma_0}\sigma_p(t;\omega,\gamma_0). \quad (1)$$

where σ_c is corrected stress, σ_p is apparent stress by PP geometry, and γ_0 is strain amplitude. Eq. (1) was successfully implemented on gluten gels and entangled polymer melt (Bharadwaj and Ewoldt, 2015; Ng *et al.*, 2011). In this study, Eq. (1) was applied to more various systems containing melts, solutions, blend, nanocomposite, and suspensions. The corrected stress requires partial derivative form of the apparent stress. To this end, several stress responses at different strain amplitudes can be used for a numerical calculation. However, potential experimental error might be expanded by such a numerical approach.

In general, oscillatory shear stress response under LAOS flow can be expressed by two types of equations (Hyun *et al.*, 2011). The nonlinear viscoelastic stress is expanded as an infinite Fourier series with the higher odd harmonics (Giacomin and Dealy, 1993).

$$\sigma(t;\omega,\gamma_0)=\gamma_0\sum_{n,\text{odd}}^{\infty}\left[G_n'(\omega,\gamma_0)\sin(n\omega t)+G_n''(\omega,\gamma_0)\cos(n\omega t)\right]. \quad (2)$$

It is also possible to write the shear stress as a power series expansion in frequency and strain amplitude (Pearson and Rochefort, 1982).

$$\sigma(t;\omega,\gamma_0)=\sum_{n,\text{odd}}^{\infty}\sum_{m,\text{odd}}^{n}\gamma_0^n\left[G'_{nm}(\omega)\sin(m\omega t)+G''_{nm}(\omega)\cos(m\omega t)\right]. \tag{3}$$

Eq. (3) separates the frequency dependence from the strain amplitude dependence, which makes the power series coefficients independent of strain amplitude. On the contrary, Fourier coefficients in Eq. (2) are functions of both frequency and strain amplitude. Comparing Eqs. (2) and (3) gives the relationship between Fourier moduli and coefficients of power series expansion as

$$\begin{aligned}
G'_1(\omega,\gamma_0)&=G'_{11}(\omega)+G'_{31}(\omega)\gamma_0^2+G'_{51}(\omega)\gamma_0^4+O(\gamma_0^6),\\
G''_1(\omega,\gamma_0)&=G''_{11}(\omega)+G''_{31}(\omega)\gamma_0^2+G''_{51}(\omega)\gamma_0^4+O(\gamma_0^6),\\
G'_3(\omega,\gamma_0)&=\quad G'_{33}(\omega)\gamma_0^2+G'_{53}(\omega)\gamma_0^4+O(\gamma_0^6),\\
G''_3(\omega,\gamma_0)&=\quad G''_{33}(\omega)\gamma_0^2+G''_{53}(\omega)\gamma_0^4+O(\gamma_0^6),\\
G'_5(\omega,\gamma_0)&=\qquad G'_{55}(\omega)\gamma_0^4+O(\gamma_0^6),\\
G''_5(\omega,\gamma_0)&=\qquad G''_{55}(\omega)\gamma_0^4+O(\gamma_0^6).
\end{aligned} \tag{4}$$

The relative third-harmonic and fifth-harmonic intensities ($I_{3/1}$ and $I_{5/1}$) can be defined by using Eq. (4).

$$\begin{aligned}
I_{3/1}(\omega,\gamma_0)&\equiv\frac{|G_3^*|}{|G_1^*|}=\frac{\sqrt{G_3'^2+G_3''^2}}{\sqrt{G_1'^2+G_1''^2}}\\
&=\frac{\sqrt{\left\{G'_{33}\gamma_0^2+G'_{53}\gamma_0^4+O(\gamma_0^6)\right\}^2+\left\{G''_{33}\gamma_0^2+G''_{53}\gamma_0^4+O(\gamma_0^6)\right\}^2}}{\sqrt{\left\{G'_{11}+G'_{31}\gamma_0^2+G'_{51}\gamma_0^4+O(\gamma_0^6)\right\}^2+\left\{G''_{11}+G''_{31}\gamma_0^2+G''_{51}\gamma_0^4+O(\gamma_0^6)\right\}^2}}\\
&=\frac{\sqrt{G'^2_{33}+G''^2_{33}+O(\gamma_0^2)}}{\sqrt{G'^2_{11}+G''^2_{11}+O(\gamma_0^2)}}\cdot\gamma_0^2,
\end{aligned} \tag{5}$$

$$
\begin{aligned}
I_{5/1}(\omega,\gamma_0) &\equiv \frac{\left|G_5^*\right|}{\left|G_1^*\right|} = \frac{\sqrt{G_5'^2+G_5''^2}}{\sqrt{G_1'^2+G_1''^2}} \\
&= \frac{\sqrt{\left\{G_{55}'\gamma_0^4+O\left(\gamma_0^6\right)\right\}^2+\left\{G_{55}''\gamma_0^4+O\left(\gamma_0^6\right)\right\}^2}}{\sqrt{\left\{G_{11}'+G_{31}'\gamma_0^2+G_{51}'\gamma_0^4+O\left(\gamma_0^6\right)\right\}^2+\left\{G_{11}''+G_{31}''\gamma_0^2+G_{51}''\gamma_0^4+O\left(\gamma_0^6\right)\right\}^2}} \\
&= \frac{\sqrt{G_{55}'^2+G_{55}''^2+O\left(\gamma_0^2\right)}}{\sqrt{G_{11}'^2+G_{11}''^2+O\left(\gamma_0^2\right)}}\cdot\gamma_0^4.
\end{aligned}
\tag{6}
$$

Therefore, $I_{3/1}$ and $I_{5/1}$ scale as γ_0^2 and γ_0^4 in MAOS regime, respectively. From these scaling relations, additional nonlinear parameters can be defined.

$$
Q_3(\omega,\gamma_0) \equiv \frac{I_{3/1}}{\gamma_0^2} = \frac{\sqrt{G_{33}'^2+G_{33}''^2+O\left(\gamma_0^2\right)}}{\sqrt{G_{11}'^2+G_{11}''^2+O\left(\gamma_0^2\right)}}, \tag{7}
$$

$$
Q_5(\omega,\gamma_0) \equiv \frac{I_{5/1}}{\gamma_0^4} = \frac{\sqrt{G_{55}'^2+G_{55}''^2+O\left(\gamma_0^2\right)}}{\sqrt{G_{11}'^2+G_{11}''^2+O\left(\gamma_0^2\right)}}. \tag{8}
$$

To obtain single-point corrections for LAOS response, Eqs. (2) and (3) can be inserted in Eq. (1) under an assumption that the nonlinear shear stress of materials is described well by Eqs. (2) or (3). The right-hand side of Eq. (1) involves the partial derivative of stress signal. Fourier moduli of Eq. (2) have the dependency on both frequency and strain amplitude, which make difficulty in mathematical calculation for partial derivative with respect to strain amplitude because in general, Fourier moduli cannot be specified analytically for any materials. Thus, power series expansion of Eq. (3) was inserted to the right-hand side of Eq. (1). For n^{th} order powers of the strain amplitude, single-point correction factors are obtained as

n = 1 (SAOS): $\sigma_{\text{c}} = \sigma_{\text{p}}$, $G_{11,\text{c}}' = G_{11,\text{p}}'$, and $G_{11,\text{c}}'' = G_{11,\text{p}}''$ (9)

n = 3 (MAOS): $\sigma_{\text{c}} = 1.5\sigma_{\text{p}}$, $G_{3k,\text{c}}' = 1.5G_{3k,\text{p}}'$, and $G_{3k,\text{c}}'' = 1.5G_{3k,\text{p}}''$ (k = 1, 3) (10)

n = 5 (LAOS): $\sigma_c = 2\sigma_p$, $G'_{5k,c} = 2G'_{5k,p}$, and $G''_{5k,c} = 2G''_{5k,p}$ (k = 1, 3, 5) (11)

The subscripts, c and p, indicate corrected and apparent properties, respectively. Using the relations of Eq. (4), the corrected Fourier moduli is also expressed.

$$\begin{aligned}
G'_{1,c}(\omega,\gamma_0) &= G'_{11,c}(\omega) + 1.5G'_{31,c}(\omega)\gamma_0^2 + 2G'_{51,c}(\omega)\gamma_0^4 + O(\gamma_0^6),\\
G''_{1,c}(\omega,\gamma_0) &= G''_{11,c}(\omega) + 1.5G''_{31,c}(\omega)\gamma_0^2 + 2G''_{51,c}(\omega)\gamma_0^4 + O(\gamma_0^6),\\
G'_{3,c}(\omega,\gamma_0) &= 1.5G'_{33,c}(\omega)\gamma_0^2 + 2G'_{53,c}(\omega)\gamma_0^4 + O(\gamma_0^6),\\
G''_{3,c}(\omega,\gamma_0) &= 1.5G''_{33,c}(\omega)\gamma_0^2 + 2G''_{53,c}(\omega)\gamma_0^4 + O(\gamma_0^6),\\
G'_{5,c}(\omega,\gamma_0) &= 2G'_{55,c}(\omega)\gamma_0^4 + O(\gamma_0^6),\\
G''_{5,c}(\omega,\gamma_0) &= 2G''_{55,c}(\omega)\gamma_0^4 + O(\gamma_0^6).
\end{aligned} \tag{12}$$

By definition, $I_{3/1}$ and Q_3 have the shift factor of 1.5 and $I_{5/1}$ and Q_5 the shift factor of 2 in the MAOS regime.

The above single-point correction approach uses vertical shifting of PP measurements only. An alternative approach is to adjust the shear rate at the rim (radius R) to match a corresponding value in CP flow, which means horizontal shifting (Giacomin *et al.*, 2015; Wilhelm *et al.*, 1999). Giacomin *et al.* (2015) derived the shear rate correction for shear-thinning power-law fluids.

$$\frac{\dot{\gamma}_{CP}}{\dot{\gamma}_R} = \left[\frac{3}{3+n}\right]^{1/n} \tag{13}$$

where $\dot{\gamma}_{CP}$ is the homogeneous shear rate in CP flow, $\dot{\gamma}_R$ is the apparent shear rate in PP flow, and n is the shear thinning index (< 1). For shear-thinning power-law fluids, the correction factor is bounded by

$$\frac{1}{\sqrt[3]{e}} \le \frac{\dot{\gamma}_{CP}}{\dot{\gamma}_R} \le \frac{3}{4} \tag{14}$$

For the special case of a Newtonian fluid, the shear rate correction gives 3/4.

3. Experimental

3.1. Single-phase system

3.1.1. Homopolymer melt and solution

Isotactic polypropylene (PP) (grade HP562T, M_n = 56,000 g/mol, M_w = 157,000 g/mol, PDI = 2.81) was obtained from PolyMirae Company Ltd. Two different polystyrene (PS) were used. Polydisperse linear PS (grade HF2680, M_n = 59,200 g/mol, M_w = 168,700 g/mol, PDI = 2.85) was provided from Samsung Cheil Industries Inc. Monodisperse linear PS (M_n = g/mol, M_w = g/mol, PDI =) was synthesized by anionic polymerization. We labeled PP and PS as PP562T, PS2680, and PS139k, respectively.

Commented [HYS1]: 교수님께서 PS139k 의 정보를 채워주셨으면 합니다.

As a homopolymer solution, monodisperse linear PS (M_n = 275,781 g/mol, M_w = 297,757 g/mol, PDI = 1.07) was dissolved in dioctyl phthalate (DOP) with 20% mass concentration. DOP is a θ solvent for PS at the θ temperature of 22°C. Tetrahydrofuran (THF), a good solvent for PS, was added as a co-solvent to facilitate mixing and ensure homogeneity of solutions. The mixture was stirred at room temperature for 1 day. THF was gradually removed by vacuum evaporation without substantial DOP loss although a small loss of DOP was inevitable. We labeled this PS solution as PS300_20.

3.1.2. Xanthan gum solution

Xanthan gum (grade G1253) was obtained from Sigma-Aldrich Inc. In this work, seven xanthan gum solutions with concentrations of 0.5, 0.8, 1, 1.5, 2, 3, and 4 wt% were prepared by slowly adding the required amount of polymer powder weighed using an electronic balance into a known volume deionized water filled in a glass container, which was maintained at 65°C with constant stirring for 4 h until the polymer was perfectly dissolved. During stirring, the

glass container was sealed up with an air-tight film to prevent evaporation. In order to complete hydration of the polymer, the prepared solutions were kept at rest at room temperature for more than 12 h prior to conducting rheological measurements.

3.2. Multiphase system

3.2.1. Polymer blend and nanocomposite

PP562T and PS2680 were mixed for PP/PS (80/20) blend system. They were dried in a vacuum oven at 80°C for 12 h and then mixed using a Haake mixer at 50 rpm and 200°C for 5 min. For nanocomposite system, 5 wt% cloisite20A (C20A) was mixed with PP562T. C20A, purchased from Southern Clay Products Inc., is a dimethyl-hydrogenated tallow ammonium-modified montmorillonite with a density of 1.77 g/cm^3. C20A was kept in a convection oven at 100°C to remove excess amount of moistures. The dried constituents were simultaneously mixed at 180°C and 100 rpm for 7 min.

3.2.2. Suspension

Poly(ethylene oxide) (PEO) and LUDOX HS-30 colloidal silica were purchased from Sigma-Aldrich Inc. The molecular weight of PEO was 600,000 g/mol. LUDOX HS-30 colloidal silica contained 30 wt% of spherical silica nanoparticles (SiNPs) of diameter of 15 nm in deionized (DI) water. PEO powder was dissolved in DI water at 40°C by magnetic stirring at 200 rpm. SiNPs were dropwisely added to aqueous PEO solution during stirring time and the mixture was homogenized for 12 h. Based on the total mass of PEO, DI water, and SiNPs, three different PEO/SiNP suspensions were prepared and labeled with concentration in wt% as PEO/SiNP (2/25), PEO/SiNP (3/20), and PEO/SiNP (3/25).

3.3. Rheological measurements

In this study, two strain-controlled rheometers, RDA Ⅱ (Rheometrics Inc.) and ARES-G2 (TA Instruments Inc.), were used to compare effects of parallel-plate (PP) and cone-plate (CP) geometries. 25-mm sized geometries were used for RDA Ⅱ and 40-mm sized geometries for ARES-G2. Cone angle of CP geometry was 0.1 and 0.04 rad for RDA Ⅱ and ARES-G2, respectively. Melt measurements were conducted with forced convection oven (FCO) at various temperatures, 180°C for PP562T and PS139k, 200°C for PS2680 and PP/PS (80/20) blend, and 170°C for PP/C20A nanocomposite. Solution measurements were carried out at 25°C with advanced peltier system (APS). Linear rheological properties were obtained through frequency sweep tests under small amplitude oscillatory shear (SAOS) flow. On the other hand, large amplitude oscillatory shear (LAOS) tests were conducted via strain sweep measurements to get nonlinear rheological responses.

4. Results and Discussion

4.1. SAOS data correction

Frequency sweep tests were carried out to evaluate linear rheological properties of the intended materials at small amplitude oscillatory shear (SAOS) flow. Experiment conditions are demonstrated in the Experimental section. Figure 2 compares the linear rheological response of single-phase systems including homogeneous melts and solution and xanthan gum solutions for PP and CP geometries. Alvarez *et al.* (2007) investigated the geometry effects on dynamic oscillatory shear flow of mashed potatoes. The lower values in case of CP geometry were reported at all temperatures and gap sizes compared with PP geometry. However, our results show that the linear viscoelastic measurements with CP and PP fixtures coincide well within experimental range of frequency and confirm that, in the linear viscoelastic regime, no shifting, horizontally or vertically, is required for PP geometry as expected by a general single-point correction of Eq. (1).

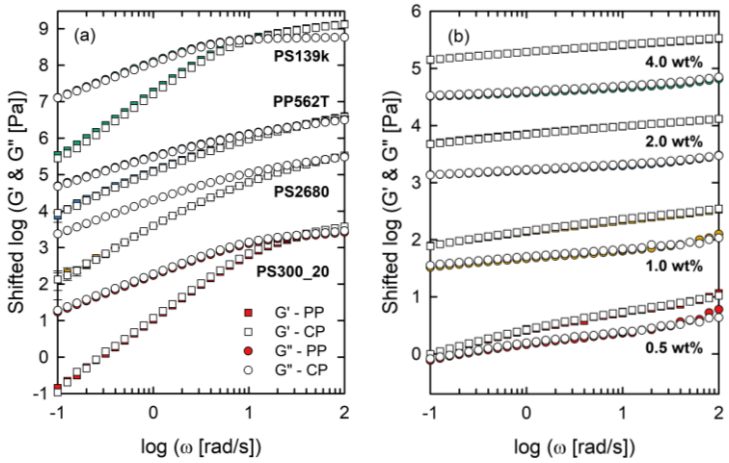

Fig. 2. Comparison of linear viscoelastic properties of single-phase systems at SAOS flow for parallel-plate (PP – filled symbols) and cone-plate (CP – open symbols) geometries. For (a) homogeneous melts and solution, each modulus has been artificially shifted by 10^0 (PS300_20), 10^1 (PS2680), 10^2 (PP562T), and 10^4 (PS139k) for the sake of clarity. For (b) xanthan gum solutions, each modulus has been shifted by 10^0 (0.5 wt%), 10^1 (1.0 wt%), 10^2 (2.0 wt%), and 10^3 (4.0 wt%), respectively.

Figure 3 shows the effect of inhomogeneous strain field of PP geometry on SAOS measurements of multiphase systems. Along with the single-phase systems, multiphase systems also display good coincidence between CP and PP measurements even though PP/PS (80/20) blend exhibits small deviations between CP and PP measurements (Fig. 3a). The PP data of PP/PS (80/20) blend are relatively lower than the CP data. This result is in agreement with those of Egres and Wagner (2005) and Shaw and Liu (2006) where they believed it as a result of errors due to wall slip effects or gap setting problems. However, taken together, no significant differences are observed in both single-phase and multiphase systems when two geometries are compared. It is reinforced that the prediction of Eq. (1) was obtained from a generalized approach. To compensate for remained differences between two geometries, PP data were vertically shifted to CP data using complex modulus, and the corresponding shift factors (V_{G^*}) are summarized in Table 2.

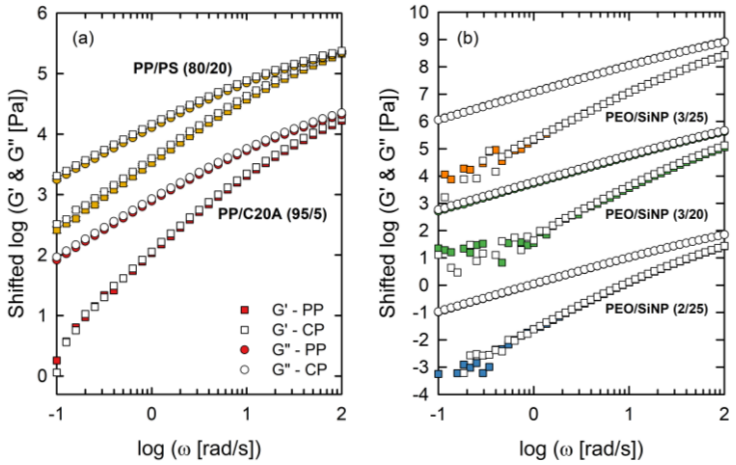

Fig. 3. Comparison of linear viscoelastic properties of multi-phase systems at SAOS flow for parallel-plate (PP – filled symbols) and cone-plate (CP – open symbols) geometries. For (a) polymer blend and nanocomposite, each modulus has been artificially shifted by 10^0 (PP/C20A) and 10^1 (PP/PS) for the sake of clarity. For (b) PEO/SiNP suspensions, each modulus has been shifted by 10^0 (2/25), 10^4 (3/20), and 10^7 (3/25).

Table 2. Vertical shift factors used in SAOS data of single-phase and multiphase systems.

Sample name	V_{G^*} [Pa]
PS300_20	1.09
PS2680	1.00
PS139k	1.00
PP562T	0.94
XG 0.5wt%	1.05
XG 0.8wt%	1.09
XG 1.0wt%	1.04
XG 1.5wt%	1.01
XG 2.0wt%	0.99
XG 3.0wt%	0.99
XG 4.0wt%	1.01
PP/C20A (95/5)	1.13
PP/PS (80/20)	1.08
PEO/SiNP (2/25)	1.02
PEO/SiNP (3/20)	1.11
PEO/SiNP (3/25)	0.99
Average	1.03 ± 0.05

4.2. LAOS data correction

To probe differences in two geometries at higher deformations, large amplitude oscillatory shear (LAOS) tests were carried out via strain sweep tests. Details of the experiment conditions are shown in the Experimental section. LAOS tests were carried out at different frequencies to compare the effect of geometries at different frequencies. Differences in PP and CP geometries on LAOS flow of 1 rad/s are compared for homopolymer melts and solution and multiphase systems in Figs. 4 and 5. Corrections for xanthan gum solutions are discussed in the next section.

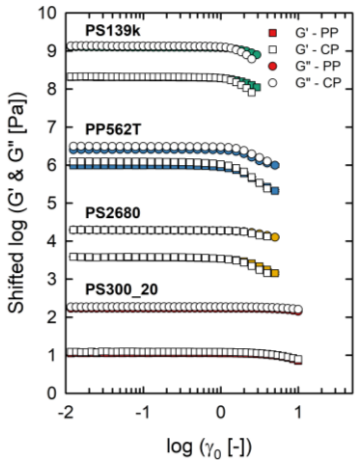

Fig. 4. Comparison of first-harmonic Fourier moduli of homopolymer melts and solution under LAOS flow for parallel-plate (PP – filled symbols) and cone-plate (CP – open symbols) geometries. The moduli have been artificially shifted by 10^0 (PS300_20), 10^1 (PS2680), 10^3 (PP562T), and 10^5 (PS139k) for the sake of clarity.

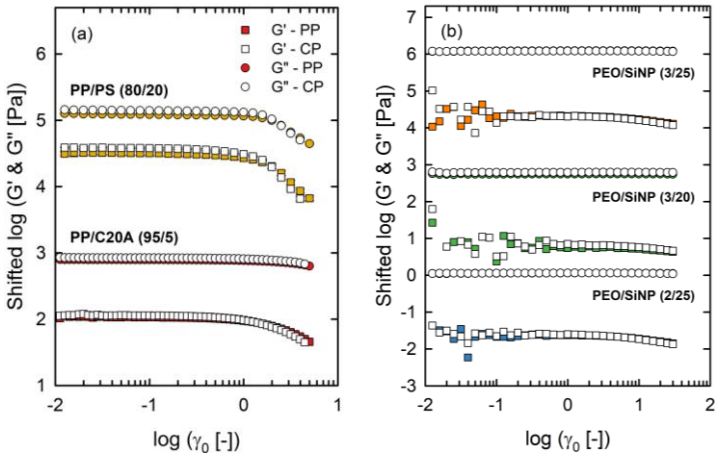

Fig. 5. Comparison of first-harmonic Fourier moduli of multiphase systems under LAOS flow for parallel-plate (PP – filled symbols) and cone-plate (CP – open symbols) geometries. For (a) polymer blend and nanocomposite, the moduli have been artificially shifted by 10^0 (PP/C20A) and 10^2 (PP/PS) for the sake of clarity. For (b) PEO/SiNP suspensions, the moduli have been shifted by 10^0 (2/25), 10^3 (3/20), and 10^6 (3/25).

In the linear regime, the first-harmonic Fourier moduli (G' and G'') by CP and PP geometries overlap reasonably even though PP562T melt and PP/PS (80/20) blend display small deviations which might be induced by wall slip effects or gap setting problems (Egres and Wagner, 2005; Shaw and Liu, 2006). As strain amplitude goes toward the nonlinear regime, both measurements start to decrease but the reduction in CP measurements is more remarkable. The decrease rate in CP is faster than in PP. The same effect is observed when samples were sheared at different frequencies (Fig. 6a). In general, PP geometry softens the first-harmonic nonlinearities (*e.g.* G'_{31}, G''_{31}, G'_{51}, and G''_{51} in Eq. (4)) and leads to small overestimation of the first-harmonic Fourier moduli. This is because part of the sample still remains in the linear regime at small radial position but nonlinear behavior already occurs at the edge of the plate

(de Souza Mendes *et al.*, 2014; Ewoldt *et al.*, 2010). Thus, all first-harmonic nonlinearities measured by PP should be vertically corrected to match CP responses. Validity of this vertical shifting was experimentally verified for two first-harmonic intrinsic nonlinearities (G'_{31} and G''_{31}) in MAOS regime by using 1.5 correction factor predicted by a single-point correction (Eq. (10)) (Bharadwaj and Ewoldt, 2015). However, for the other first-harmonic nonlinearities higher than third order, such vertical shifts have not been reported yet. In addition, it is impossible to calculate the infinite number of first-harmonic nonlinearities from experiments. Another method to perform vertical shifting is to calculate the partial derivative of PP stress response in Eq. (1) by numerical techniques such as a centered difference method at each instant in time (Ng *et al.*, 2011). However, it contains much tedious calculation at all instant time and such numerical techniques can magnify any experimental error. Instead, we used horizontal shifting approach because PP and CP data can be superposed by only one shift process. The corresponding shift factors (H_{G^*}) are summarized in Table 3, with vertical shift factors (V_{G^*}) to compensate for remained differences between CP and PP data. Figure 6b shows that the horizontal shift gives good superposition of the first-harmonic Fourier moduli between CP and PP geometries. The $H_{G^*} < 1$ in Table 3 confirms again that nonlinear behavior is observed faster in CP fixture. The horizontal shifts used in this section might not be explained by shear rate correction theory of Giacomin *et al.* (2015) because the maximum correction factor in shear rate correction is 0.75 of a Newtonian fluid limit whereas the experimental average value is 0.89. We lastly highlight that each coefficient of power series expansion is corrected by the vertical shifting of the single-point correction but the first-harmonic Fourier moduli, which have complex relationship as Eq. (4), are properly corrected by the horizontal shifting.

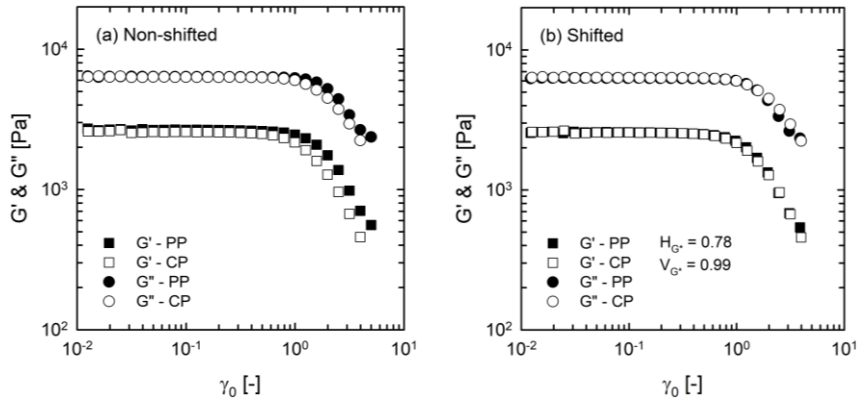

Fig. 6. First-harmonic moduli (G' and G'') of PS2680 melt as a function of strain amplitude at 5 rad/s and 200°C for parallel plate (PP – filled symbols) and cone plate (CP – open symbols). (a) Raw results and (b) shifted results by horizontal and vertical shift factors (0.78 and 0.99).

FT-rheology was used to investigate shift factors of nonlinear parameters defined in the Theory section ($I_{3/1}$, Q_3, $I_{5/1}$, and Q_5). First, $I_{3/1}$ and Q_3 are plotted as a function of strain amplitude in Fig. 7 for PS2680 melt. We obtained theoretically the vertical shift factor of 1.5 from the single-point correction. Figure 7 shows that single vertical shift factor is enough to superpose $I_{3/1}$ and Q_3 between CP and PP and that no horizontal shifting is needed. The obtained vertical shift factors (V_{Q_3}) are listed in Table 3. The experimentally-determined shift factors are identical to the theoretical value of 1.5 within measurement uncertainty, which agrees with the result of Giacomin *et al.* (2015) and reinforces validity of the single-point correction method. Simultaneously, $Q_{3,0}$ parameter, an asymptotic value of Q_3 at low strain amplitude, can be corrected by the value of 1.5, as applied to homopolymer systems (Song *et al.*, 2016; Song *et al.*, 2017; Wagner *et al.*, 2011). Small amount of deviations might be explained by wall slip effects or gap setting problems (Egres and Wagner, 2005; Shaw and Liu, 2006). Giacomin *et al.* (2015) derived differences of $I_{3/1}$ between CP and PP measurements as functions of

frequency and strain rate amplitude using a single-mode corotational Maxwell model. The model expression for $I_{3/1}$ (Eq. (50) in their paper) displays a constant value of 1.5 at Wi ($\equiv \lambda\gamma_0\omega$) < 0.1 and becomes a function of strain rate amplitude at Wi > 0.1. Experimental condition of PS2680 in Fig. 7 gives Wi = 5.83 at γ_0 = 1. However, the experimental data still exhibit good superposition. It is speculated that the vertical shifting is enough for CP and PP data to be superposed.

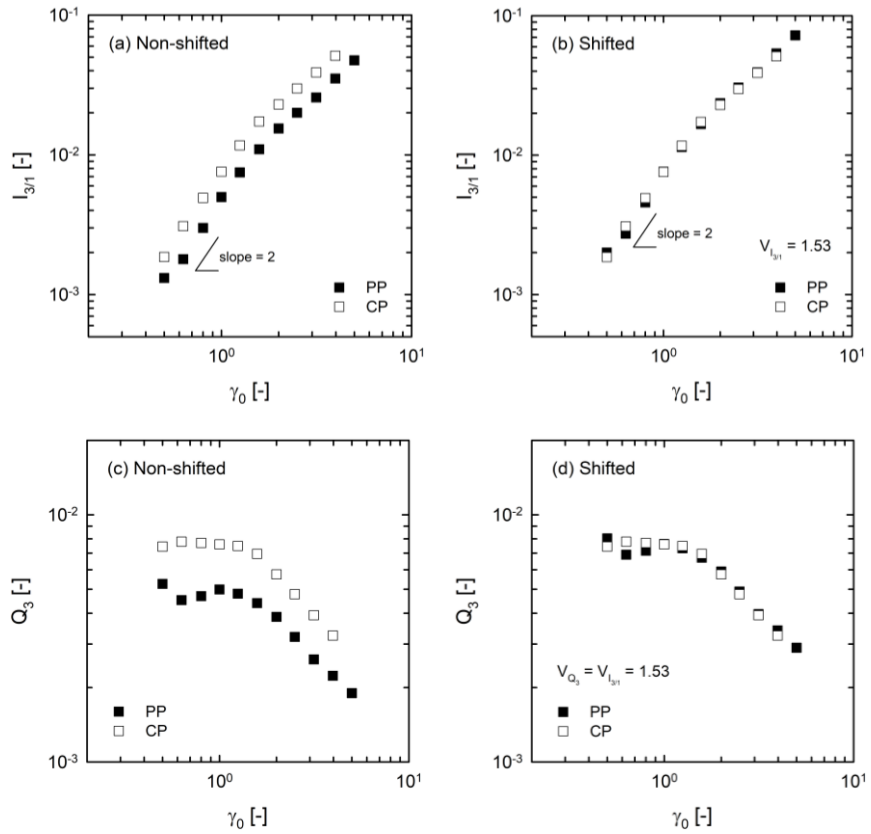

Fig. 7. Relative third-harmonic intensity ($I_{3/1}$) and nonlinear parameter (Q_3) of PS2680 melt as a function of strain amplitude at 5 rad/s and 200°C for parallel plate (PP – filled symbols) and cone plate (CP – open symbols). (a), (c) Non-shifted and (b), (d) shifted results by vertical shift factor only.

Correction factors of $I_{5/1}$ and Q_5 are investigated in Fig. 8 and summarized in Table 3. Compared with $I_{3/1}$ and Q_3, $I_{5/1}$ and Q_5 do not display clear scaling behaviors at low strain amplitude ($I_{5/1} \propto \gamma_0^4$ and plateau for Q_5). It is difficult to obtain reliable LAOS data higher than the third harmonic because experimental artifacts such as edge fracture and wall slip frequently occur at larger strain amplitudes and (Hyun *et al.*, 2011). Thus, vertical shifting was evaluated for some of samples used. The obtained correction factors for $I_{5/1}$ and Q_5 exhibit larger deviations with the theoretical value of 2 than those for $I_{3/1}$ and Q_3. However, considering possible experimental difficulties mentioned above, the correction factor of $I_{5/1}$ and Q_5 looks indeed 2. The same result was obtained using a corotational Maxwell model (Giacomin *et al.*, 2015). In addition, $Q_{5,0}$ parameter, an asymptotic value of Q_5 at low strain amplitude, can be corrected by the value of 2 if the data display a plateau behavior in the plot of Q_5 as a function of strain amplitude.

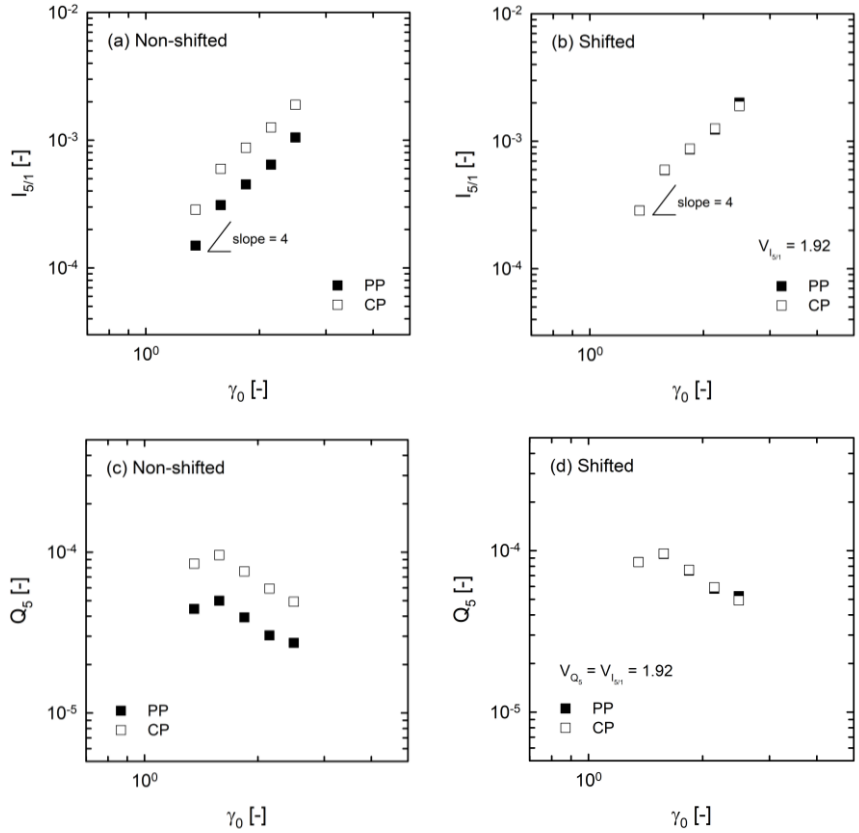

Fig. 8. Relative fifth-harmonic intensity ($I_{5/1}$) and nonlinear parameter (Q_5) of PS300_20 solution as a function of strain amplitude at 6.3 rad/s and 25°C for parallel plate (PP – filled symbols) and cone plate (CP – open symbols). (a), (c) Non-shifted and (b), (d) shifted results by vertical shift factor only.

Table 3. Horizontal and vertical shift factors used in LAOS data of homopolymer melts and solution and multiphase systems.

Sample name	Test frequency [rad/s]	H_{G^*} [-]	V_{G^*} [Pa]	V_{Q_3} [-]	V_{Q_5} [-]
PS300_20	1	0.90	1.09	1.42	2.06
	1.6	0.97	1.07	1.40	1.83
	2.5	0.95	1.05	1.40	1.84
	4	0.92	1.03	1.39	1.76
	6.3	0.89	1.03	1.43	1.92
	10	0.95	1.02	1.44	1.90
PS2680	1	0.85	1.03	1.53	-
	5	0.78	0.99	1.53	2.01
PS139k	1	0.85	1.07	1.56	-
	3	0.70	1.05	1.43	-
	5	0.91	1.05	1.50	-
	7	0.94	1.06	1.56	-
PP562T	1	0.92	1.23	1.48	-
	2	0.95	1.00	1.58	-
	3	0.90	1.02	1.48	-
	5	0.87	0.99	1.50	-
PP/C20A (95/5)	1	0.92	1.06	1.38	1.81
PP/PS (80/20)	1	0.88	1.14	1.60	-
	5	0.87	1.02	1.48	1.88
PEO/SiNP (2/25)	1	0.84	1.00	1.42	-
PEO/SiNP (3/20)	1	0.86	1.13	1.52	-
PEO/SiNP (3/25)	1	0.82	1.00	1.37	-
Average		0.88 ± 0.06	1.05 ± 0.05	1.47 ± 0.07	1.89 ± 0.09

4.3. Vertical and horizontal shifting in xanthan gum solutions

We now focus on shift factors used in nonlinear rheological properties of xanthan gum solutions. As the previous section, we start a discussion with the first-harmonic Fourier moduli. Non-shifted storage and loss moduli (G' and G'') are plotted as a function of strain amplitude in Fig. 9. Here again, samples measured by CP geometry display a little larger storage and loss moduli within linear regime compared with PP geometry. The distinguished effect of homogeneity of flow field is observed at loss modulus of 1.0 wt% solution. The CP-measured loss modulus exhibits a weak strain overshoot, indicating LAOS type Ⅲ. On the contrary, the PP-measured loss modulus exhibits a strain thinning, indicating LAOS type Ⅰ (Hyun *et al.*, 2002). Xanthan gum is a non-gelling biopolymer but a gel-like structure is present in concentrated xanthan gum solutions (Song *et al.*, 2006). In addition, the maximum overshoot peak of G'' in 4 wt% solution has a larger value in PP measurement than in CP measurement (83.4 Pa in PP and 101.65 Pa in CP). For materials showing a gel-like response, the usage of CP geometry seems necessary to capture nonlinear rheological properties exactly. Both moduli are shifted horizontally and vertically to correct PP measurements as shown in Fig. 10 and the corresponding shift factors are listed in Table 5. The results show good agreement between CP and PP measurements except near a strain overshoot in G''.

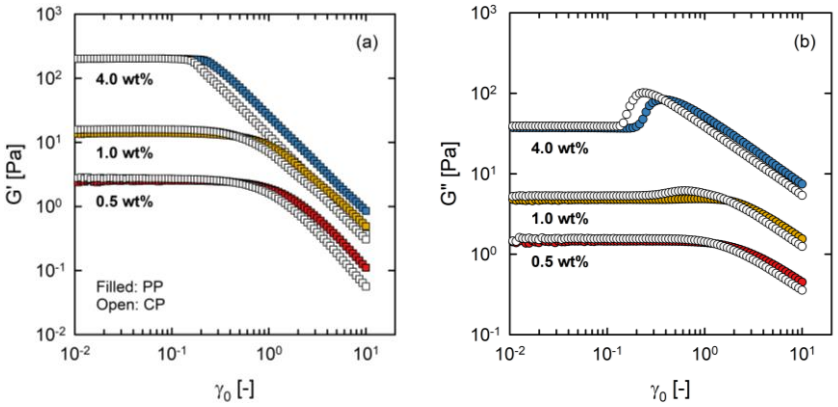

Fig. 9. Non-shifted first-harmonic (a) storage and (b) loss moduli of xanthan gum solutions with 0.5, 1, and 4 wt% concentrations under LAOS flow at 1 rad/s and 25°C for parallel-plate (PP – filled symbols) and cone-plate (CP – open symbols) geometries.

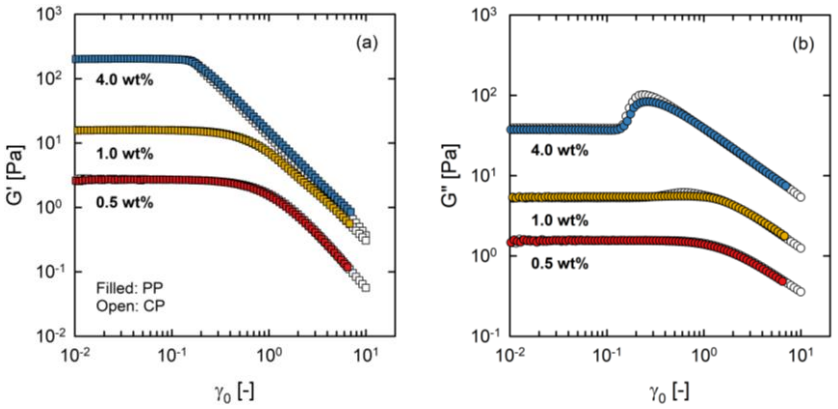

Fig. 10. Shifted first-harmonic (a) storage and (b) loss moduli of xanthan gum solutions with 0.5, 1, and 4 wt% concentrations under LAOS flow at 1 rad/s and 25°C for parallel-plate (PP – filled symbols) and cone-plate (CP – open symbols) geometries. The horizontal and vertical shift factors are listed in Table 5.

Xanthan gum has been known to a highly shear thinning behavior originating from its unique rigid, rod-like conformation. In an aqueous solution at 25°C, backbone of xanthan gum is disordered but highly extended. Due to the highly extended structure, it is more responsive to shear than a general polymer melt or solution which has a random-coil conformation (Hyun *et al.*, 2003; Song *et al.*, 2006). Complex viscosity of xanthan gum solutions used was plotted in Fig. 11 to reveal the highly shear thinning property. The data were fitted by power-law type equation ($\eta^* = a\omega^{n-1}$) and resultant shear thinning index (n) is listed in Table 4. Giacomin *et al.* (2015) derived shear rate correction factor as a function of shear thinning index for shear-thinning power-law fluids (Eq. (13) in the Theory section). Because xanthan gum solutions display a shear thinning following power law behavior, theoretical shear rate correction factor was calculated by Eq. (13) and summarized in Table 4. Interestingly, the calculated values agree with the average value of experimentally-determined horizontal shift factors within standard deviations. It is speculated that the horizontal shifting in xanthan gum solutions is related to shear rate correction approach of Eq. (13).

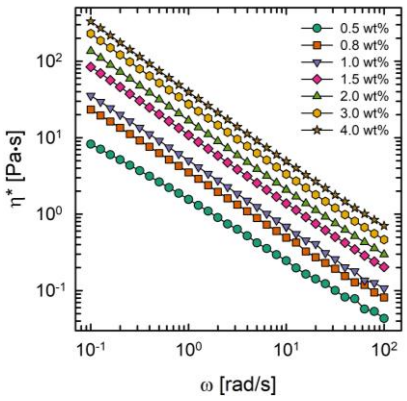

Fig. 11. Complex viscosity of xanthan gum solutions as a function of frequency at 25°C.

Table 4. Shear thinning index (n) of xanthan gum solution and corresponding shear rate correction factor calculated by Eq. (13).

Concentration [wt%]	n [-]	$\dot{\gamma}_{CP}/\dot{\gamma}_R$ [-]
0.5	0.208	0.724
0.8	0.179	0.723
1.0	0.153	0.722
1.5	0.111	0.721
2.0	0.094	0.720
3.0	0.078	0.720
4.0	0.076	0.719

We mentioned that first-harmonic Fourier moduli measured with PP are also corrected vertically at each strain amplitude by a single-point correction approach instead of the use of one horizontal shift factor. In Fig. 12, stress responses of 4 wt% xanthan gum solution are presented at two different strain amplitudes. For PP correction, partial derivative of stress signal in Eq. (1) was numerically calculated from a centered finite difference formula. At $\gamma_0 = 0.2$, PP response lies in a transition from linear to nonlinear regime while CP response already displays nonlinear behavior. At $\gamma_0 = 8.0$, both responses display intercycle strain softening behavior (see Fig. 9). The corrected stress at $\gamma_0 = 8.0$ shows a good agreement with the CP-measured stress. However, the situation is totally reversed at $\gamma_0 = 0.2$. The CP response is highly distorted but the PP and corrected responses look sinusoidal. Similar phenomenon was observed in Lissajous curves of elastic Bingham model (Ewoldt *et al.*, 2010). At extremely low or high strain amplitudes, both homogeneous and inhomogeneous strains produce the same Lissajous patterns. When the maximum stress starts to exceed the yield stress under homogeneous strain (*e.g.* $\sigma_{max}/\sigma_Y = 1.001$), the model exhibits plastic behavior. However, at the same maximum stress under inhomogeneous strain, most of the model response is still in the unyielded regime although strain amplitude at the edge of PP plate might move to the yielded regime. Thus, a

general single-point correction, which vertically shifts PP measurements, cannot explain the effect of inhomogeneous flow properly in shear-thinning power-law fluids or yield stress fluids. Instead, shear rate correction method can be an adequate solution.

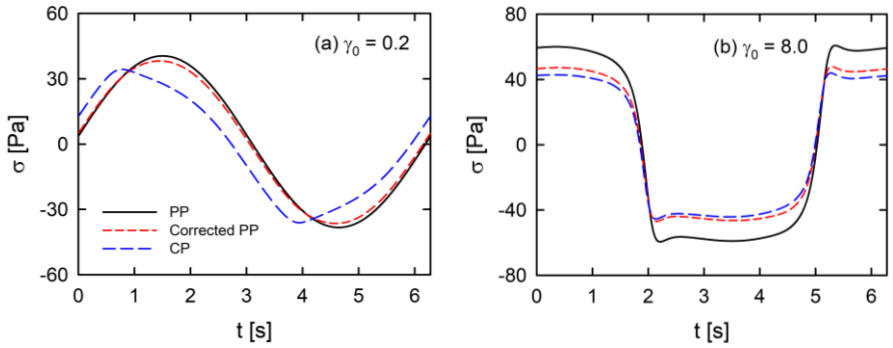

Fig. 12. Stress response of 4 wt% xanthan gum solutions measured by CP (blue color) and PP (black color) at 1 rad/s and 25°C. The PP data corrected by a single-point correction are red-colored.

Table 5. Horizontal and vertical shift factors used in first-harmonic Fourier moduli of xanthan gum solutions.

Concentration [wt%]	Test frequency [rad/s]	H_{G^*} [-]	V_{G^*} [Pa]
0.5	1	0.65	1.07
	3	0.73	1.04
	5	0.74	1.04
	7	0.72	1.05
	10	0.72	1.06
0.8	1	0.71	1.10
	3	0.69	1.12
	5	0.71	1.10
	7	0.73	1.13
	10	0.69	1.14

1.0	1	0.68	1.14
	3	0.73	1.14
	5	0.70	1.11
	7	0.73	1.07
	10	0.76	1.04
1.5	1	0.63	1.00
	3	0.71	1.03
	5	0.72	1.00
	7	0.75	1.00
	10	0.80	1.07
2.0	1	0.65	1.11
	3	0.80	1.08
	5	0.69	1.09
	7	0.80	1.13
	10	0.71	1.08
3.0	1	0.60	1.03
	3	0.76	1.02
	5	0.72	1.05
	7	0.74	1.05
	10	0.77	1.30
4.0	1	0.70	1.00
	3	0.74	1.00
	5	0.71	1.03
	7	0.75	1.00
	10	0.75	1.00
Average		0.72 ± 0.04	1.07 ± 0.06

The shear rate correction was applied to four nonlinear parameters, $I_{3/1}$, Q_3, $I_{5/1}$, and Q_5. In Figs. 13 and 14, non-shifted and shifted $I_{3/1}$ and Q_3 are given as a function of strain amplitude. All correction factors used for $I_{3/1}$ and Q_3 of xanthan gum solutions are listed in Table 6. Although a single vertical shift factor of about 1.5 is able to superpose $I_{3/1}$ and Q_3 measured by CP and PP for materials used in the previous section, the superposition is achieved by using a horizontal shift factor as well as a vertical shift factor, in case of xanthan gum solutions. The xanthan gum solution of 0.5 wt% concentration, which displays a strain thinning of LAOS type Ⅰ (Hyun *et al.*, 2002), obtains perfect superposition of $I_{3/1}$ with a horizontal shift factor accounting for shear rate correction (averagely 0.72) and a small vertical shift factor (Figs. 13a and b). Unlike the systems in the previous section where the superposition of $I_{3/1}$ and Q_3 was obtained by vertical shift factors only, a horizontal shift factor has a dominant contribution to the superposition of $I_{3/1}$ of 0.5 wt% xanthan gum solution. In case of Q_3 superposition, it needs a large vertical shift factor as well as the same horizontal shift factor as used for $I_{3/1}$ (Figs. 13c and d). It is rationalized by definition of Q_3.

$$V_{Q_3} Q_3 = \frac{V_{I_{3/1}} I_{3/1}}{\left(H_{I_{3/1}} \gamma_0\right)^2} = \frac{V_{I_{3/1}}}{H_{I_{3/1}}^2} \cdot \frac{I_{3/1}}{\gamma_0^2}, \tag{15}$$

where V_{Q_3} is a vertical shift factor for Q_3 and $H_{I_{3/1}}$ and $V_{I_{3/1}}$ are a horizontal and vertical shift factor for $I_{3/1}$. From Eq. (15), $V_{Q_3} = V_{I_{3/1}} / H_{I_{3/1}}^2$. The experimentally-determined and calculated values are almost identical (*e.g.* V_{Q_3} = 2.12 and $V_{I_{3/1}} / H_{I_{3/1}}^2$ = 2.12 at 1 rad/s). Thus, the obtained correction factors are reasonable. The xanthan gum solution with 4 wt% concentration also exhibits good agreement between CP and PP data with both horizontal and vertical shift factors, except a strain overshoot regime in Q_3 (Fig. 14). The difference between overshoot peaks of CP and PP measurements is observed in xanthan gum solutions displaying LAOS type Ⅲ in the first-harmonic moduli (1, 1.5, 2, 3, and 4 wt%). The higher loss modulus peak in CP

measurement is not perfectly attenuated even after vertical shifting. Because the dominant contribution near this overshoot of Q_3 is viscous nonlinearity (not shown here), Q_3 parameter displays a strain overshoot and a similar deviation of overshoot peaks between CP and PP results.

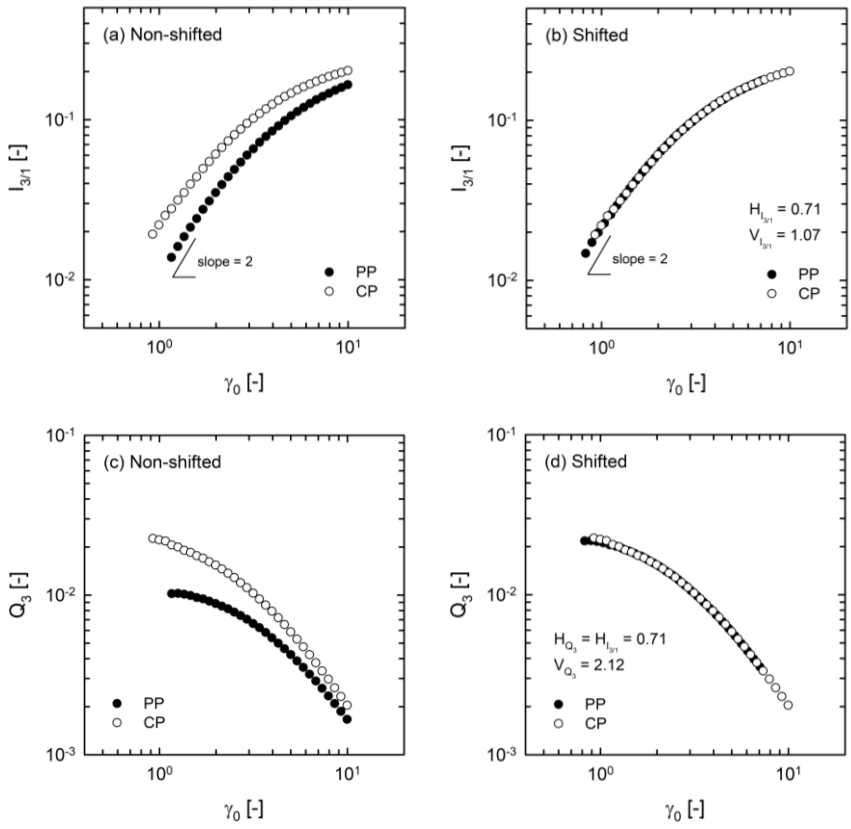

Fig. 13. Relative third-harmonic intensity ($I_{3/1}$) and nonlinear parameter (Q_3) of 0.5 wt% xanthan gum solution as a function of strain amplitude at 1 rad/s and 25°C for parallel plate (PP – filled symbols) and cone plate (CP – open symbols). (a), (c) Non-shifted and (b), (d) shifted results by horizontal and vertical shift factors.

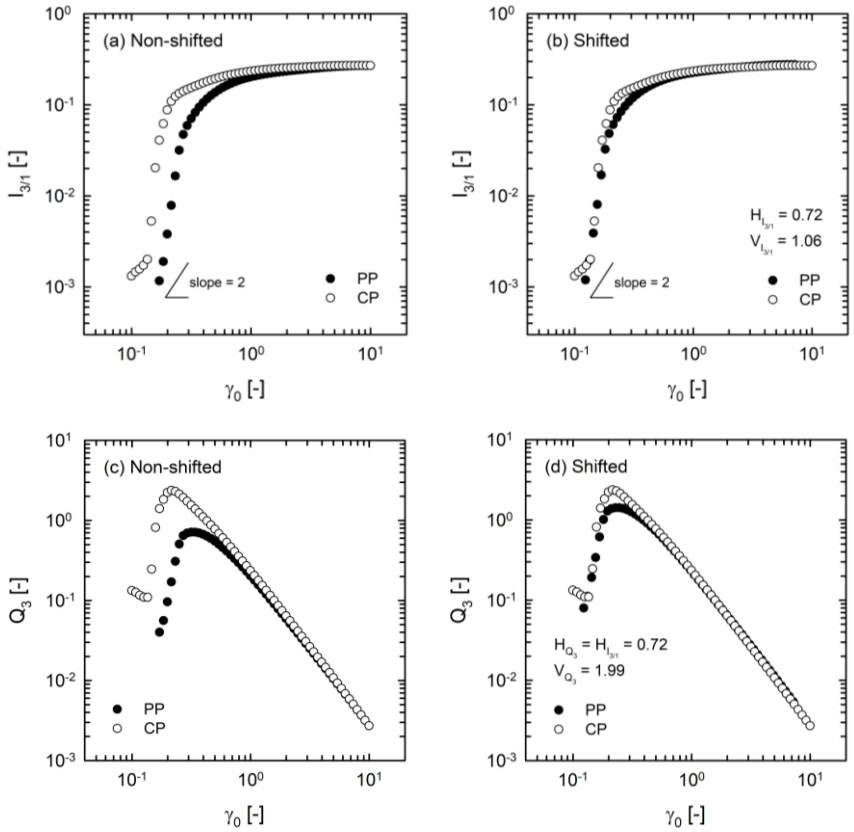

Fig. 14. Relative third-harmonic intensity ($I_{3/1}$) and nonlinear parameter (Q_3) of 4 wt% xanthan gum solution as a function of strain amplitude at 1 rad/s and 25°C for parallel plate (PP – filled symbols) and cone plate (CP – open symbols). (a), (c) Non-shifted and (b), (d) shifted results by horizontal and vertical shift factors.

The same method was applied to $I_{5/1}$ and Q_5 of xanthan gum solutions. Likewise, the superposition of $I_{5/1}$ and Q_5 is achieved by using a horizontal shift factor as well as a vertical shift factor although a single vertical shift factor of about 2 is able to superpose $I_{5/1}$ and Q_5 measured by CP and PP for materials used in the previous section. The xanthan gum solutions of LAOS type Ⅰ display a perfect superposition of $I_{5/1}$ and Q_5 with both horizontal and vertical

shift factors, as $I_{3/1}$ and Q_3 in Fig. 13. However, the solutions of LAOS type Ⅲ display a deviation at overshoot point of Q_5 due to the same reason as for Q_3 (Fig. 15). All correction factors used for $I_{5/1}$ and Q_5 of xanthan gum solutions are listed in Table 6. Interestingly, all horizontal shift factors used in first-harmonic Fourier moduli and FT-based nonlinear parameters are averagely 0.72, which reinforces the importance of shear rate correction in shear-thinning power-law fluids or yield stress fluids. From superposition for Q_5, the average vertical shift factor is 4.11. It is also rationalized by definition of Q_5.

$$V_{Q_5} Q_5 = \frac{V_{I_{5/1}} I_{5/1}}{\left(H_{I_{5/1}} \gamma_0\right)^2} = \frac{V_{I_{5/1}}}{H_{I_{5/1}}^2} \cdot \frac{I_{5/1}}{\gamma_0^2}. \tag{16}$$

Thus, $V_{Q_5} = V_{I_{5/1}} / H_{I_{5/1}}^2$. The experimentally-determined and calculated values are almost identical (*e.g.* V_{Q_5} = 4.44 and $V_{I_{5/1}} / H_{I_{5/1}}^2$ = 4.41 at 1 rad/s for 0.5 wt% solution). Again, the obtained correction factors are reasonable.

One interesting point should be addressed. The general single-point correction of Eq. (10) gives vertical shift factors of 1.5 for Q_3 and 2 for Q_5. However, the experimentally-determined values for all xanthan gum solutions are averagely 2.11 for Q_3 and 4.10 for Q_5 (Table 6). One possibility is a violation of odd-harmonic strain amplitude scaling of $I_{3/1}$ and $I_{5/1}$ in the MAOS regime. Recently, for some thixotropic models, even-harmonic or non-integer strain amplitude scaling was reported (*e.g.* $I_{3/1} \propto \gamma_0^1$) (Blackwell and Ewoldt, 2014; Blackwell and Ewoldt, 2016). The shift factors of 2.11 for Q_3 and 4.10 for Q_5 correspond to scaling exponents of 5.44 and 13.4, respectively. ($I_{3/1} \propto \gamma_0^{5.44}$ and $I_{5/1} \propto \gamma_0^{13.4}$). Thus, even-harmonic or non-integer strain amplitude scaling cannot be the reason for such differences. Another possibility is an invalidity of a power-series expression of nonlinear shear stress in xanthan gum solutions. Vertical stress correction by the single-point correction is still valid except the points where CP measurement exhibits nonlinear response while PP measurement lies in the linear regime,

as shown in Fig. 12. Thus, the failure in prediction is from usage of a power-series expansion of stress response. That is, nonlinear shear stress of xanthan gum solutions might not be explained by a power-series expansion. However, it is difficult to draw any definite conclusion at this level. We just leave it as a future work.

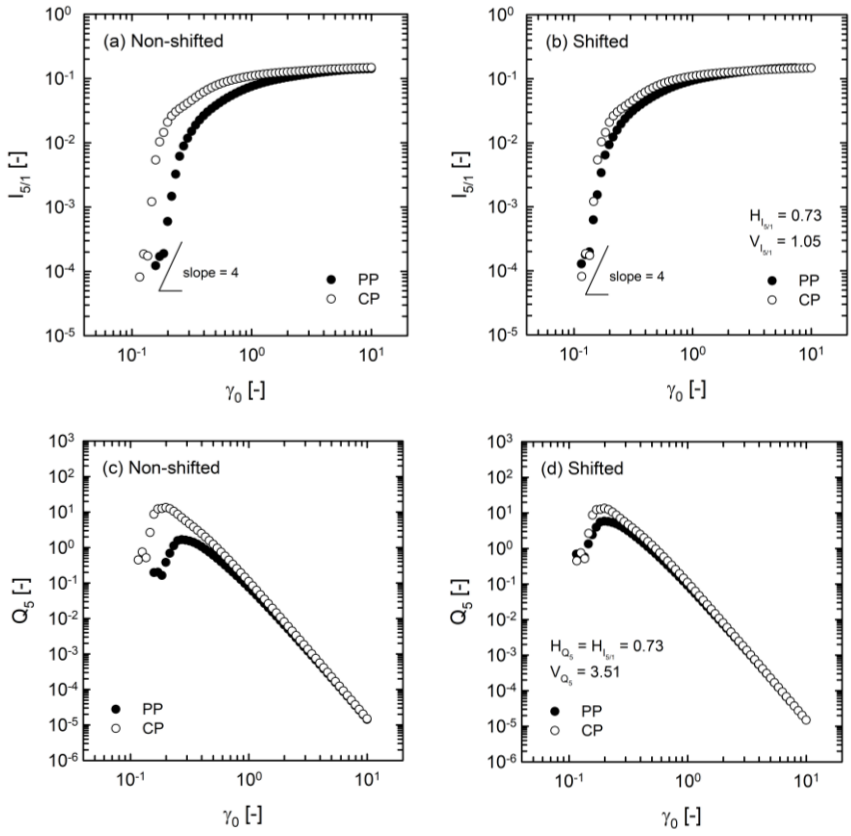

Fig. 15. Relative fifth-harmonic intensity ($I_{5/1}$) and nonlinear parameter (Q_5) of 4 wt% xanthan gum solution as a function of strain amplitude at 1 rad/s and 25°C for parallel plate (PP – filled symbols) and cone plate (CP – open symbols). (a), (c) Non-shifted and (b), (d) shifted results by horizontal and vertical shift factors.

Table 6. Horizontal and vertical shift factors used in FT-based nonlinear parameters of xanthan gum solutions.

Concentration [wt%]	Test frequency [rad/s]	$H_{I_{3/1}}$ [-]	$V_{I_{3/1}}$ [-]	V_{Q_3} [-]	$H_{I_{5/1}}$ [-]	$V_{I_{5/1}}$ [-]	V_{Q_5} [-]
0.5	1	0.71	1.07	2.12	0.70	1.06	4.44
	3	0.70	1.06	2.17	0.73	1.11	3.88
	5	0.73	1.10	2.05	0.73	1.11	4.02
	7	0.73	1.10	2.09	0.73	1.16	4.02
	10	0.72	1.11	2.11	0.74	1.20	3.90
0.8	1	0.72	1.08	2.10	0.72	1.15	4.27
	3	0.73	1.10	2.04	0.73	1.17	4.08
	5	0.73	1.08	2.02	0.72	1.14	4.14
	7	0.73	1.08	2.01	0.72	1.14	4.08
	10	0.71	1.06	2.12	0.73	1.23	4.33
1.0	1	0.72	1.06	2.04	0.70	1.10	4.49
	3	0.70	1.06	2.11	0.73	1.12	4.00
	5	0.72	1.08	2.11	0.72	1.08	4.08
	7	0.72	1.07	2.13	0.72	1.07	4.10
	10	0.72	1.08	2.07	0.71	1.06	4.20
1.5	1	0.72	1.33	2.60	0.78	1.79	4.91
	3	0.65	1.24	2.98	0.77	1.61	4.58
	5	0.74	1.16	2.07	0.74	1.29	4.22
	7	0.73	1.08	1.93	0.72	1.13	4.02
	10	0.79	1.02	1.40	0.75	1.00	2.94
2.0	1	0.60	1.02	2.80	0.72	1.12	4.10
	3	0.73	1.03	1.89	0.72	1.03	3.878
	5	0.72	1.03	2.00	0.72	1.12	4.20
	7	0.87	1.01	1.29	0.71	1.00	3.65
	10	0.71	1.08	2.10	0.71	1.09	4.14
3.0	1	0.57	1.17	3.61	0.73	1.25	4.33
	3	0.70	1.08	2.24	0.73	1.22	4.08

	5	0.74	1.06	1.98	0.73	1.19	4.08
	7	0.73	1.00	1.70	0.73	1.11	4.00
	10	0.74	1.00	1.71	0.71	1.00	3.81
4.0	1	0.72	1.06	1.99	0.73	1.05	3.51
	3	0.70	1.07	2.18	0.70	1.15	4.60
	5	0.74	1.10	1.96	0.71	1.12	4.24
	7	0.72	1.08	2.01	0.71	1.12	4.24
	10	0.71	1.06	2.10	0.73	1.12	3.86
Average		0.72 ± 0.04	1.08 ± 0.06	2.11 ± 0.39	0.72 ± 0.02	1.15 ± 0.15	4.10 ± 0.33

5. Conclusion

A comparative study of rheological properties of various complex fluids from single-phase to multiphase systems for parallel-plate (PP) and cone-plate (CP) geometries was conducted. Linear and nonlinear rheological properties were measured using strain-controlled SAOS and LAOS tests.

Two theoretical approaches were adopted: a general single-point correction and a shear rate correction. A general single-point correction shifts nonlinear data vertically at a fixed strain amplitude whereas a shear rate correction shifts them horizontally. Theoretical predictions were validated with strain-controlled SAOS and LAOS experiments. It was confirmed that within linear regime of strain sweep results, CP- and PP-measured first-harmonic moduli coincide with each other. As nonlinear behavior is generated, vertical and horizontal shift factors are required. For all systems except xanthan gum solutions, first-harmonic Fourier moduli are perfectly superposed by use of one horizontal shift factor of averagely 0.88. Four FT-based nonlinear parameters ($I_{3/1}$, Q_3, $I_{5/1}$, and Q_5) need only vertical shift factor. $I_{3/1}$ and Q_3 measured by PP are vertically shifted by multiplying 1.47 averagely. $I_{5/1}$ and Q_5 are corrected vertically by the average value of 1.89. These experimentally-determined values are identical to the theoretical values of 1.5 and 2 by the single-point correction within a standard deviation.

On the contrary, xanthan gum solutions display anomalous corrections in nonlinear data. The first-harmonic Fourier moduli are superposed by a horizontal shift factor, as the other systems. However, smaller value of 0.72 is obtained, which corresponds to the prediction by shear rate correction. In contrast with the other systems, $I_{3/1}$ and $I_{5/1}$ of xanthan gum solutions are corrected by horizontal shift factors. Q_3 and Q_5 are corrected by both horizontal and vertical shift factors. The obtained vertical values for Q_3 and Q_5 (2.11 and 4.10) are larger than the theoretical values of the single-point correction (1.5 and 2), which indicates a possibility that

nonlinear stress response of xanthan gum solutions might not be explained by a power-series expansion. This finding for xanthan gum solutions reinforces the importance of shear rate correction in shear-thinning power-law fluids or yield stress fluids.

Acknowledgement

This research was supported by the Global Ph.D. Fellowship Program (2014H1A2A1015767) and the Basic Science Research Program (2015R1D1A1A09057413) through the National Research Foundation of Korea (NRF) funded by the Ministry of Education.

References

Alvarez, M.D., W. Canet, and C. FernÁNdez, 2007, THE EFFECT OF TEMPERATURE, GEOMETRY, GAP AND SURFACE FRICTION ON OSCILLATORY RHEOLOGICAL PROPERTIES OF MASHED POTATOES, *J. Food Process Eng.* **30**, 267-292.

Bharadwaj, N.A. and R.H. Ewoldt, 2015, Single-point parallel disk correction for asymptotically nonlinear oscillatory shear, *Rheol. Acta* **54**, 223-233.

Blackwell, B.C. and R.H. Ewoldt, 2014, A simple thixotropic–viscoelastic constitutive model produces unique signatures in large-amplitude oscillatory shear (LAOS), *J. Non-Newt. Fluid Mech.* **208**, 27-41.

Blackwell, B.C. and R.H. Ewoldt, 2016, Non-integer asymptotic scaling of a thixotropic-viscoelastic model in large-amplitude oscillatory shear, *J. Non-Newt. Fluid Mech.* **227**, 80-89.

Bohlin, L., T.L.G. Carlson, and G. Bäckström, 1980, Cone-plate instrument for stress relaxation measurements, *J. Colloid Interf. Sci.* **73**, 61-65.

Carvalho, M.S., M. Padmanabhan, and C.W. Macosko, 1994, Single- point correction for parallel disks rheometry, *J. Rheol.* **38**, 1925-1936.

de Souza Mendes, P.R., A.A. Alicke, and R.L. Thompson, 2014, Parallel-plate geometry correction for transient rheometric experiments, *Appl. Rheol.* **24**, 52721.

Djalili-Moghaddam, M., R. Ebrahimzadeh, and S. Toll, 2004, Study of geometry effects in torsional rheometry of fibre suspensions, *Rheol. Acta* **44**, 29-37.

Egres, R.G. and N.J. Wagner, 2005, The rheology and microstructure of acicular precipitated calcium carbonate colloidal suspensions through the shear thickening transition, *J. Rheol.* **49**, 719-746.

Ewoldt, R.H., 2013, Defining nonlinear rheological material functions for oscillatory shear, *J. Rheol.* **57**, 177-195.

Ewoldt, R.H. and N.A. Bharadwaj, 2013, Low-dimensional intrinsic material functions for nonlinear viscoelasticity, *Rheol. Acta* **52**, 201-219.

Ewoldt, R.H., P. Winter, J. Maxey, and G.H. McKinley, 2010, Large amplitude oscillatory shear of pseudoplastic and elastoviscoplastic materials, *Rheol. Acta* **49**, 191-212.

Fahimi, Z., C.P. Broedersz, T.H.S. van Kempen, D. Florea, G.W.M. Peters, and H.M. Wyss, 2014, A new approach for calculating the true stress response from large amplitude oscillatory shear (LAOS) measurements using parallel plates, *Rheol. Acta* **53**, 75-83.

Giacomin, A.J. and J.M. Dealy, 1993, Large-amplitude oscillatory shear, Springer

Giacomin, A.J., P.H. Gilbert, D. Merger, and M. Wilhelm, 2015, Large-amplitude oscillatory shear: comparing parallel-disk with cone-plate flow, *Rheol. Acta* **54**, 263-285.

Hyun, K., S.H. Kim, K.H. Ahn, and S.J. Lee, 2002, Large amplitude oscillatory shear as a way to classify the complex fluids, *J. Non-Newt. Fluid Mech.* **107**, 51-65.

Hyun, K., J.G. Nam, M. Wilhelm, K.H. Ahn, and S.J. Lee, 2003, Nonlinear response of complex fluids under LAOS (large amplitude oscillatory shear) flow, *Korea-Aust. Rheol. J.* **15**, 97-105.

Hyun, K. and M. Wilhelm, 2009, Establishing a New Mechanical Nonlinear Coefficient *Q* from FT-Rheology: First Investigation of Entangled Linear and Comb Polymer Model Systems, *Macromolecules* **42**, 411-422.

Hyun, K., M. Wilhelm, C.O. Klein, K.S. Cho, J.G. Nam, K.H. Ahn, S.J. Lee, R.H. Ewoldt, and G.H. McKinley, 2011, A review of nonlinear oscillatory shear tests: Analysis and application of large amplitude oscillatory shear (LAOS), *Prog. Polym. Sci.* **36**, 1697-1753.

Kavehpour, H.P. and G.H. McKinley, 2004, Tribo-Rheometry: From Gap-Dependent Rheology to Tribology, *Tribol. Lett.* **17**, 327-335.

Keentok, M. and R.I. Tanner, 1982, Cone- Plate and Parallel Plate Rheometry of Some Polymer Solutions, *J. Rheol.* **26**, 301-311.

Lodge, A.S., 1961, Rheological properties of concentrated polymer solutions I. Growth of pressure fluctuations during prolonged shear flow, *Polymer* **2**, 195-201.

Macosko, C.W., 1994, *Rheology: principles, measurements, and applications*, Wiley-vch

Ng, T.S.K., G.H. McKinley, and R.H. Ewoldt, 2011, Large amplitude oscillatory shear flow of gluten dough: A model power-law gel, *J. Rheol.* **55**, 627-654.

Pearson, D.S. and W.E. Rochefort, 1982, Behavior of concentrated polystyrene solutions in large- amplitude oscillating shear fields, *J. Polym. Sci., Polym. Phys. Ed.* **20**, 83-98.

Phan-Thien, N., M. Newberry, and R.I. Tanner, 2000, Non-linear oscillatory flow of a soft solid-like viscoelastic material, *J. Non-Newt. Fluid Mech.* **92**, 67-80.

Shaw, M.T. and Z.Z. Liu, 2006, Single-point determination of nonlinear rheological data from parallel-plate torsional flow, *Appl. Rheol.* **16**, 70-79.

Song, H.Y., O.S. Nnyigide, R. Salehiyan, and K. Hyun, 2016, Investigation of nonlinear rheological behavior of linear and 3-arm star 1,4-cis-polyisoprene (PI) under medium amplitude oscillatory shear (MAOS) flow via FT-rheology, *Polymer* **104**, 268-278.

Song, H.Y., S.J. Park, and K. Hyun, 2017, Characterization of Dilution Effect of Semidilute Polymer Solution on Intrinsic Nonlinearity Q_0 via FT Rheology, *Macromolecules.*

Song, K.W., H.Y. Kuk, and G.S. Chang, 2006, Rheology of concentrated xanthan gum solutions: Oscillatory shear flow behavior, *Korea-Aust. Rheol. J.* **18**, 67-81.

Soskey, P.R. and H.H. Winter, 1984, Large Step Shear Strain Experiments with Parallel- Disk Rotational Rheometers, *J. Rheol.* **28**, 625-645.

Stickel, J.J., J.S. Knutsen, and M.W. Liberatore, 2013, Response of elastoviscoplastic materials to large amplitude oscillatory shear flow in the parallel-plate and cylindrical-Couette geometries, *J. Rheol.* **57**, 1569-1596.

Wagner, M.H., V.H. Rolón-Garrido, K. Hyun, and M. Wilhelm, 2011, Analysis of medium amplitude oscillatory shear data of entangled linear and model comb polymers, *J. Rheol.* **55**, 495-516.

Wilhelm, M., P. Reinheimer, and M. Ortseifer, 1999, High sensitivity Fourier-transform rheology, *Rheol. Acta* **38**, 349-356.